Electronic Supplementary Material (ESI) for Journal of Materials Chemistry C.

Supporting information for

Impact of excess PbI_2 on the structure and the temperature dependent optical properties of $MAPbI_3$

Tobias Meier[1#], Tanaji P. Gujar[2#], Andreas Schönleber[3], Selina Olthof[4], Klaus Meerholz[4], Sander van Smaalen[3], Fabian Panzer[1], Mukundan Thelakkat[2], Anna Köhler[1,5*]

[1] Soft Matter Optoelectronics, University of Bayreuth, Bayreuth 95440, Germany.

[2] Applied Functional Polymers, Macromolecular Chemistry I, University of Bayreuth, Bayreuth 95440, Germany.

[3] Laboratory of Crystallography, University of Bayreuth, 95440 Bayreuth, Germany.

[4] Department of Chemistry, University of Cologne, Luxemburger Straße 116, Cologne 50939, Germany.

[5] Bayreuth Institute of Macromolecular Research (BIMF), University of Bayreuth, Bayreuth 95440, Germany.

# Both authors contributed equally.

Corresponding Author

[*]E-Mail: anna.koehler@uni-bayreuth.de

Solar cell parameters of $MAPbI_3$ devices

Device Fabrication

50 nm compact-TiO_2 (c-TiO_2) blocking layer was deposited by spray pyrolysis of titanium (IV) bis(acetoacetonato)-di(isopropanoxylate) diluted in ethanol at 450 °C on FTO-coated glass substrates and annealed at 450 °C for 1 h. After cooling, the substrates were transferred in a glovebox under N_2 atmosphere. For $CH_3NH_3PbI_3$ films preparation, we have used same procedure as discussed in sample preparation section. The HTL deposition solution comprised of 2,2',7,7'-tetrakis-(N,N-di-p-methoxyphenylamine) 9, 9'-spirobifluorene (spiro-OMeTAD) in chlorobenzene (102.85 mg/ml), 40 ml of 4-tert-butylpyridine and 37 ml (520 mg/ml) solution of bis(trifluoromethane) sulfonimide lithium salt (LiTFSI) in acetonitrile. This solution was spin coated at 2000 rpm for 30 s under N_2 condition and stored in dry air for overnight. No oxidants were used. This was followed by thermal deposition of gold to form the back contact. The active areas of the devices fabricated in this work are 0.09 and 0.16 cm^2.

Table S1 Photovoltaic parameters of the best performing devices prepared with different amount of excess PbI_2 in the precursor solution of $MAPbI_3$ samples. All the devices were measured directly after preparation in nitrogen atmosphere under 100 $mW.cm^{-2}$ AM 1.5 irradiation at a scan rate of 100 $mV.s^{-1}$ in reverse bias. The average value over up to 7 devices are given in brackets for all parameters.

Excess PbI_2 (mol %)	J_{SC} (mA/cm^{-2})		V_{OC} (V)		FF (%)		PCE (%)	
0	17.79	(17.21)	1.05	(1.04)	62.75	(63.3)	11.72	(11.35)
5	17.40	(16.62)	1.06	(1.05)	64.46	(62.7)	11.89	(10.93)
10	16.30	(16.01)	1.05	(1.04)	59.89	(59.07)	10.25	(9.86)
15	16.56	(16.3)	1.06	(1.06)	55.89	(54.37)	9.81	(9.37)
20	17.02	(16.53)	1.05	(1.05)	55.46	(56.35)	9.91	(9.74)
25	15.74	(15.17)	1.03	(1.03)	57.84	(57.44)	9.38	(8.95)

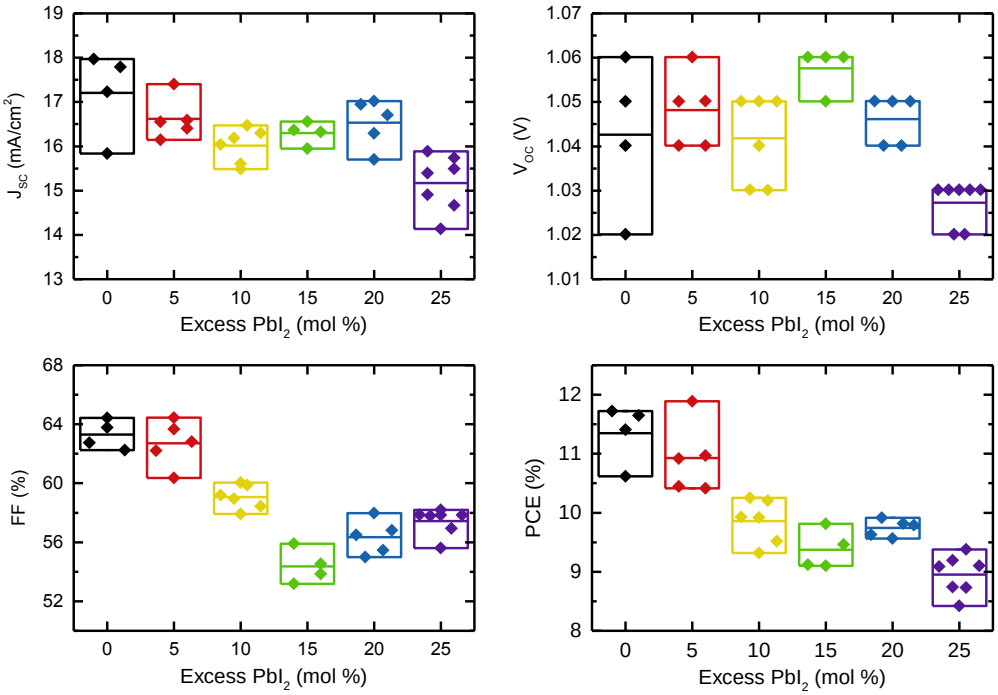

Figure S1 Short-circuit current, open-circuit voltage, fill factor and power conversion efficiencies of all investigated devices with different amount of excess PbI_2 in the precursor solution of $MAPbI_3$.

SEM images of $MAPbI_3$ samples

The average grain size of the samples with different amount of PbI_2 in the precursor solution was determined from scanning electron microscopy images (Figure S2a). The area of each individual grain was analyzed with the open source software ImageJ and values for the diameter of circles of equal area were calculated. Histograms of this analysis are shown in Figure S2b. In order to compare these values with the ones extracted from XRD the average value was calculated as a volume average reduced to length because XRD peak intensities are sensitive to the volume of the grains. In detail, the average value was taken from the third root of the average of diameters weighted with their third power.

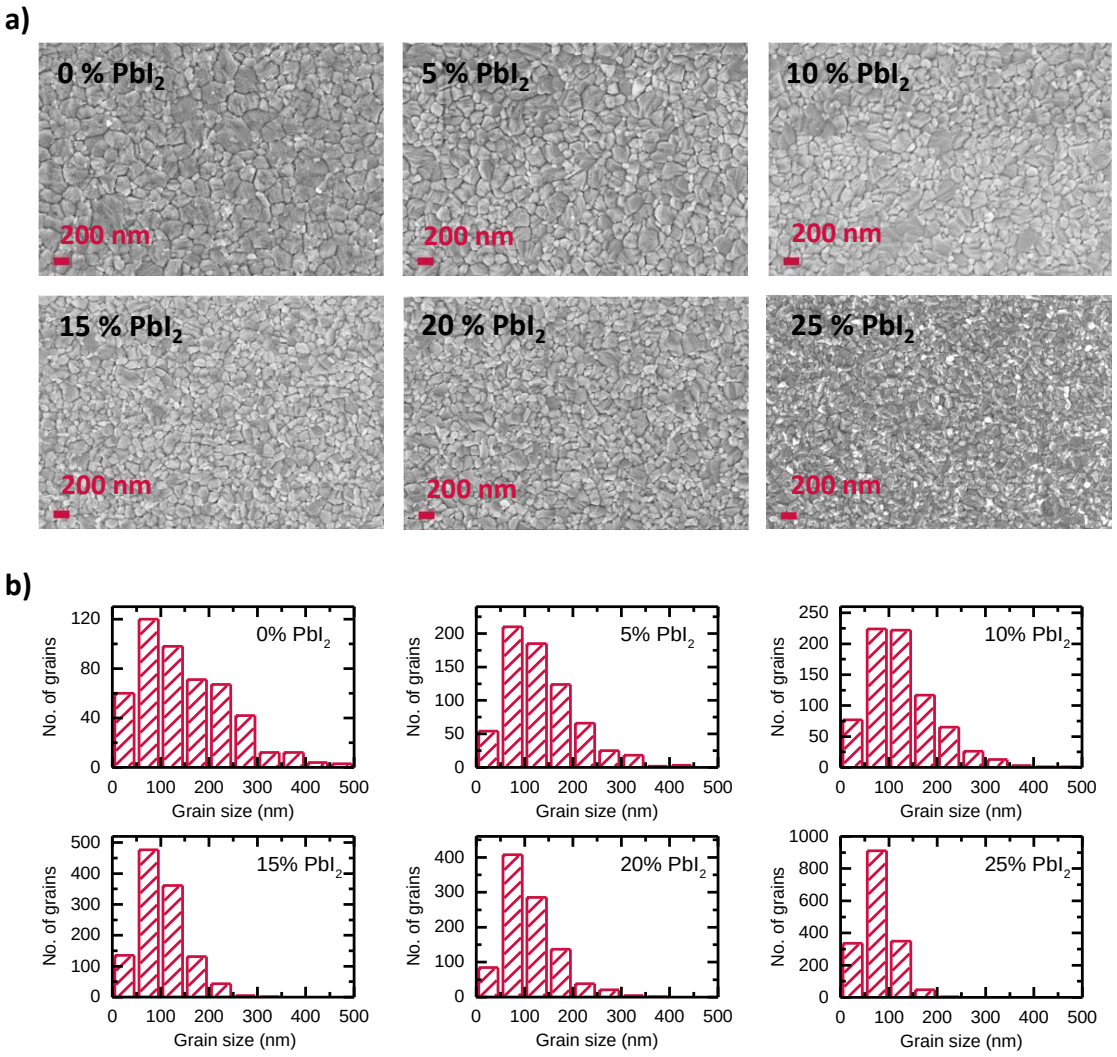

Figure S2 (a) SEM images of the investigated samples which differ in the degree of excess PbI_2 in the precursor solution. The values for the amount of excess PbI_2 are given as molar ratio. (b) Histograms showing the results of the grain size analysis for each sample.

Method to determine the percentage of PbI_2 content in $CH_3NH_3PbI_3$ by XRD

The mass ratio $\frac{x_{CH_3NH_3PbI_3}}{x_{PbI_2}}$ is proportional to the intensity ratio $\frac{I_{K,CH_3NH_3PbI_3}}{I_{L,PbI_2}}$ of the K^{th} peak of phase $CH_3NH_3PbI_3$ at diffraction angle $2\theta_K$ and the L^{th} peak of phase PbI_2 at diffraction angle $2\theta_L$ (with $\frac{v_{CH_3NH_3PbI_3}}{v_{PbI_2}}$ as volume ratio):

$$\frac{I_{K,CH_3NH_3PbI_3}}{I_{L,PbI_2}} = \left(\frac{G_{K,CH_3NH_3PbI_3}}{G_{L,PbI_2}}\right) \cdot \frac{v_{CH_3NH_3PbI_3}}{v_{PbI_2}} = \left(\frac{G_{K,CH_3NH_3PbI_3}}{G_{L,PbI_2}}\right) = \frac{\left({}^{x}/_{\rho}\right)_{CH_3NH_3PbI_3}}{\left({}^{x}/_{\rho}\right)_{PbI_2}}$$

$$\Rightarrow \quad \frac{I_{K,CH_3NH_3PbI_3}}{I_{L,PbI_2}} = \left(\frac{G_{K,CH_3NH_3PbI_3}}{G_{L,PbI_2}}\right)\left(\frac{\rho_{CH_3NH_3PbI_3}}{\rho_{PbI_2}}\right)^{-1}\left(\frac{x_{CH_3NH_3PbI_3}}{x_{PbI_2}}\right)$$

$$\Rightarrow \quad \frac{x_{CH_3NH_3PbI_3}}{x_{PbI_2}} = \left(\frac{G_{K,CH_3NH_3PbI_3}}{G_{L,PbI_2}}\right)^{-1}\left(\frac{\rho_{CH_3NH_3PbI_3}}{\rho_{PbI_2}}\right)\left(\frac{I_{K,CH_3NH_3PbI_3}}{I_{L,PbI_2}}\right)$$

with $G_i(hkl) = L_i(\theta_K) \cdot P_i(\theta_K) \cdot H_i \cdot |F_i(hkl)|^2$

- $L_i(\theta_K)$ is the Lorentz factor: $L(\theta) = \frac{1}{sin^2(\theta)\cos(\theta)}$
- $P_i(\theta_K)$ is the polarization factor for Bragg-Brentano geometry with incident beam monochromator: $P(\theta) = \frac{1+cos^2(2\theta_M)cos^2(2\theta)}{1+cos^2(2\theta_M)}$ with $2\theta_M$ as Bragg angle of the monochromator, $2\theta_M = 27{,}28°$.
- H_i is the multiplicity and $F_i(hkl)$ the structure factor of reflection hkl.

$$\frac{x_{CH_3NH_3PbI_3}}{x_{PbI_2}} = \left(\frac{L_{CH_3NH_3PbI_3}(\theta)}{L_{PbI_2}(\theta)} \cdot \frac{P_{CH_3NH_3PbI_3}(\theta)}{P_{PbI_2}(\theta)} \cdot \frac{H_{CH_3NH_3PbI_3} \cdot |F_{CH_3NH_3PbI_3}|^2}{H_{PbI_2} \cdot |F_{PbI_2}|^2}\right)^{-1}\left(\frac{\rho_{CH_3NH_3PbI_3}}{\rho_{PbI_2}}\right)\left(\frac{I_{CH_3NH_3PbI_3}}{I_{PbI_2}}\right)$$

For the phase $CH_3NH_3PbI_3$ the peak at diffraction angle $2\theta_K = 14.110°$ is used. This is a superposition of the reflections 110 (multiplicity $H = 4$, structure amplitude $F = 313$) and 002 (multiplicity $H = 2$, structure amplitude $F = 338$). For the phase PbI_2 the peak at diffraction angle $2\theta_L = 12.645°$ is used. This is reflection 001 (multiplicity $H = 2$, structure amplitude $F = 287$).

With the relation $x_{CH_3NH_3PbI_3} + x_{PbI_2} = 1$ follows then for x_{PbI_2}:

$$x_{PbI_2} = \frac{x_{PbI_2}}{x_{CH_3NH_3PbI_3} + x_{PbI_2}} = \frac{1}{\frac{x_{CH_3NH_3PbI_3}}{x_{PbI_2}} + 1}$$

Table S2 PbI_2 content in $MAPbI_3$ films for different amount of excess PbI_2 in the precursor solution calculated from XRD.

Excess PbI_2 (mol %)	rel. intensities	mass ratio $\frac{x_{CH_3NH_3PbI_3}}{x_{PbI_2}}$	PbI_2 content x_{PbI_2}
0	$I_{CH_3NH_3PbI_3} = 9.2295$ $I_{PbI_2} =$ –	100	–
5	$I_{CH_3NH_3PbI_3} = 8.0786$ $I_{PbI_2} = 0.6424$	25.6795	0.0375
10	$I_{CH_3NH_3PbI_3} = 7.7374$ $I_{PbI_2} = 1.6283$	9.7032	0.0934
15	$I_{CH_3NH_3PbI_3} = 6.8085$ $I_{PbI_2} = 1.5820$	8.7882	0.1022
20	$I_{CH_3NH_3PbI_3} = 6.5624$ $I_{PbI_2} = 1.9606$	6.8349	0.1276
25	$I_{CH_3NH_3PbI_3} = 4.4302$ $I_{PbI_2} = 2.3226$	3.8950	0.2043

Crystallite size of PbI_2 in $MAPbI_3$ samples

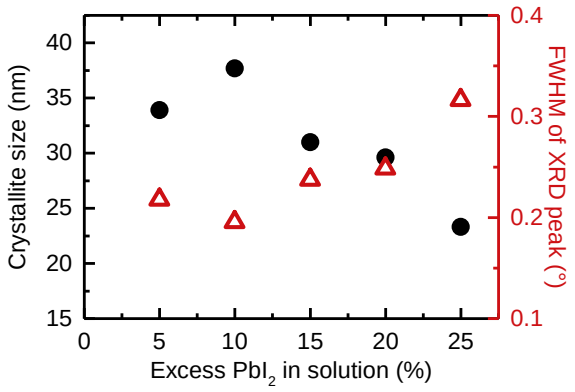

Figure S3 Crystallite size of PbI_2 (black dots) and FWHM (red triangles) of the <001> XRD peak of PbI_2 in $MAPbI_3$ thin films with different amount of excess PbI_2 in the precursor solution.

Determination of sample composition from XPS

Figure S4a and b show the core level intensities of the nitrogen 1s and lead $4f_{7/2}$ signal for 300 nm thick samples containing PbI_2 excess between 0 and 25 %. While the nitrogen signal does not significantly differ between the samples, there is a clear emergence of a second peak in the lead signal with increasing PbI_2 content. The dominant peak at 138.5 eV is due to $Pb^{(II)}$, which can be present in both $CH_3NH_3PbI_3$ and PbI_2, whereas the small emerging peak at 136.8 eV indicates the presence of metallic lead $Pb^{(0)}$. We can determine the film composition by comparing the relative intensities for the XPS peaks of nitrogen, lead and iodine, as detailed below. Figure S4c and d show the concentration of excess PbI_2 as well as metallic $Pb^{(0)}$ found in our samples using this approach. The concentrations of both PbI_2 and $Pb^{(0)}$ increase with the amount of PbI_2 in the precursor solution. For PbI_2, it becomes clear that the concentration obtained by XPS scales with the amount of excess PbI_2 in the precursor solution for ratios up to 25 mol %.

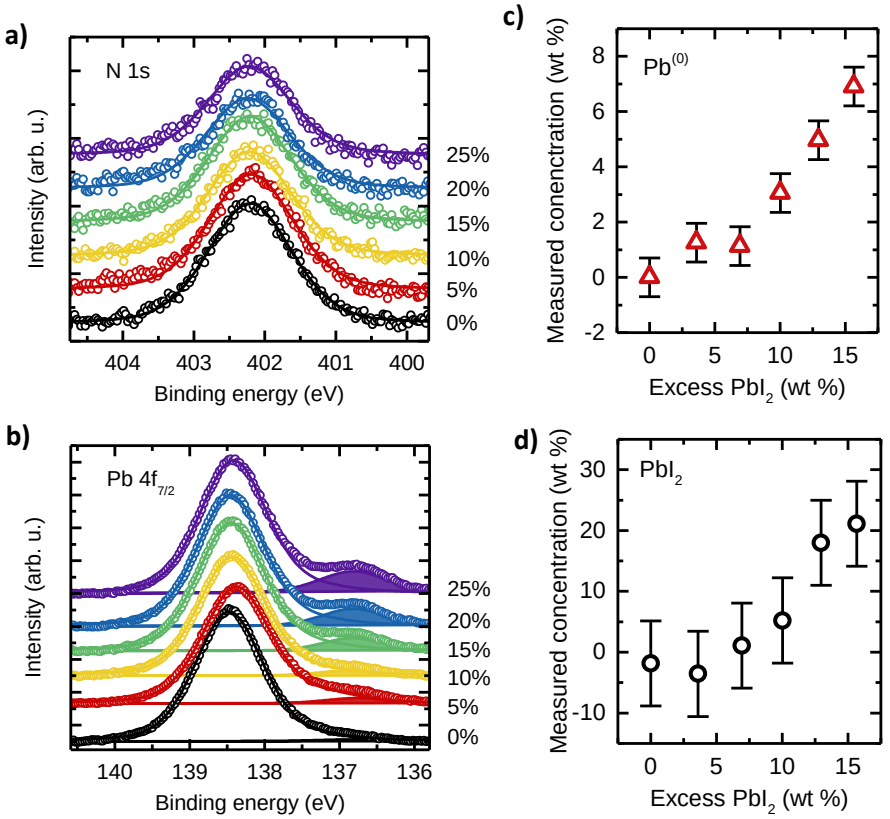

Figure S4 XPS measurements of $MAPbI_3$ films with excess PbI_2 in the precursor solution ranging from 0 % to 25 %. (a) Signal of the nitrogen 1s core level. (b) Signal of the lead $4f_{7/2}$ level. The filled area indicates metallic $Pb^{(0)}$. Concentration of (c) metallic $Pb^{(0)}$ and (d) PbI_2 present in the samples calculated from the XPS measurements.

In order to analyze how the sample composition changes upon adding additional PbI_2, the XPS core level signals were investigated. The nitrogen and lead peaks are presented in the main article, Figure 2, while Figure S4 shows the carbon and iodide peaks. Iodide $3d_{5/2}$ can be fitted by a single peak located at 618.88 eV ± 0.05 eV, which corresponds to the $I^{(-1)}$ oxidation state in either the perovskite or PbI_2 (not distinguishable). Carbon on the other hand shows the perovskite related peak at 286.2 ± 0.05 eV as well as a smaller signal of a more neutral carbon species around 284.6 eV which is likely originating from solvent remaining in or on the film.

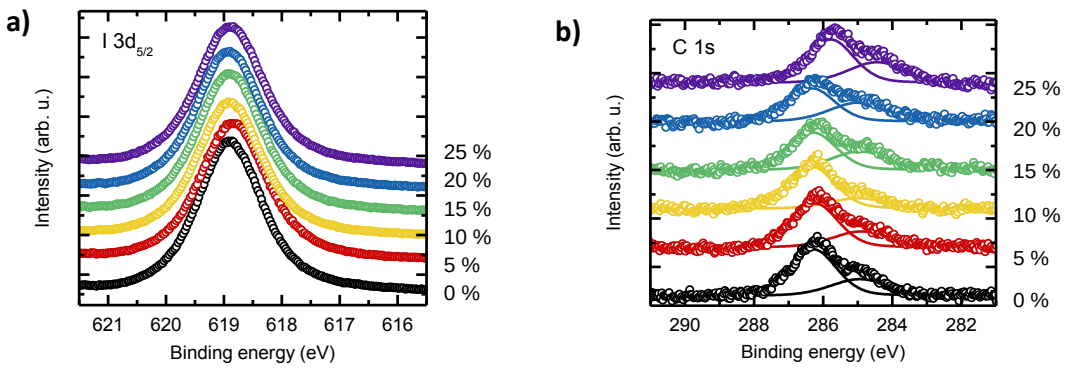

Figure S5 XPS measurements of $MAPbI_3$ films with excess PbI_2 in the precursor solution ranging from 0 mol % to 25 mol %, showing (a) the signal of the Iodide $3d_{5/2}$ core level peaks and (b) the signal of the carbon 1s level.

The core level signal of C, N, Pb, and I were fitted by mixed Gaussian/Lorentzian peaks from which the peak areas were extracted as shown in Table S3; the values presented here have already been corrected by their relative sensitivity factors (cross sections of the photo-ionization process). Next, these areas can be used to extract the layer composition, by normalizing all signals against a specific element. Here, we used nitrogen as standard (i.e. dividing all peak areas by the corresponding N 1s area), as the organic cation indicates the amount of perovskite present in the system, while both I and Pb are added via the excess PbI_2. Carbon is not a suitable indicator as the additional solvent signal makes the evaluation more error prone.

As can be seen in the middle section of Table S3, the amount of I, Pb^{+2}, and Pb^0 increases as more PbI_2 is added. The value of the excess in the right hand side of Table S3 is calculated by looking at the deviation of I^{-1} and Pb^{+2} core level signals from the expected stoichiometry C(1)N(1)Pb(1)I(3) and then averaging these results to deduce the amount of PbI_2. For low concentrations of additional PbI_2, the excess concentration is in the range of the error bars of the measurement (approximately ± 5 % in Figure S4c) which is the reason why some values even become negative here. On the other hand, the amount of metallic Pb^0 (filled peak in Figure 2, main article) can be evaluated with much higher precision of approximately ± 0.7 % as the peak is clearly separated and can be well fitted (see Figure 2 main article), so no subtraction procedure has to be performed here.

Table S3 Summary over the findings by XPS core level analysis. On the left hand side, the table shows the fitted peak area of carbon, nitrogen, lead and iodide (note: for carbon only the perovskite related peak intensity is listed). In the center the relative elemental composition is calculated by normalizing all peak areas to the nitrogen signal. On the right hand side the excess signal of I^2 and Pb^{2+} is calculated using the deviation from the expected perovskite stoichiometry. Excess values are given both in molar ratio (MR) and weight percentage.

	Measured XPS peak areas					Stoichiometry relative to N=1					Excess of …		**Average excess PbI_2** (MR) **(wt%)**
mol%	C	N	I	$Pb^{(+2)}$	$Pb^{(0)}$	C	N	$Pb^{(+2)}$	**$Pb^{(0)}$** (MR) **(wt%)**	I	I_2	Pb^{2+}	
0	879	577	2017	649	0	1.3	1	0.96	0 **0**	2.98	-0.01	-0.04	-0.02 **-1.8**
5	829	649	1909	598	25	1.29	1	0.93	0.04 **1.26**	2.96	-0.02	-0.07	-0.05 **-3.6**
10	792	588	1802	586	20	1.35	1	1	0.03 **1.13**	3.07	0.03	0	0.02 **1.1**
15	705	595	1883	630	56	1.18	1	1.07	0.09 **3.05**	3.16	0.08	0.07	0.07 **5.2**
20	629	509	1855	646	80	1.3	1	1.27	0.16 **4.97**	3.64	0.32	0.27	0.29 **18.0**
25	605	498	1896	657	111	1.21	1	1.32	0.22 **6.91**	3.8	0.40	0.32	0.36 **21.1**

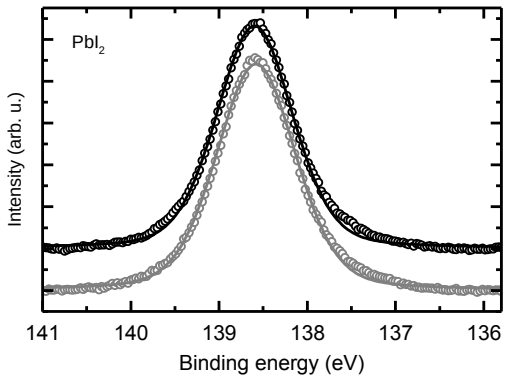

Figure S6 XPS measurement of two pure PbI_2 thin films. The signal corresponds to the lead $4f_{7/2}$ level.

Temperature dependent absorption spectra with different amount of excess PbI_2

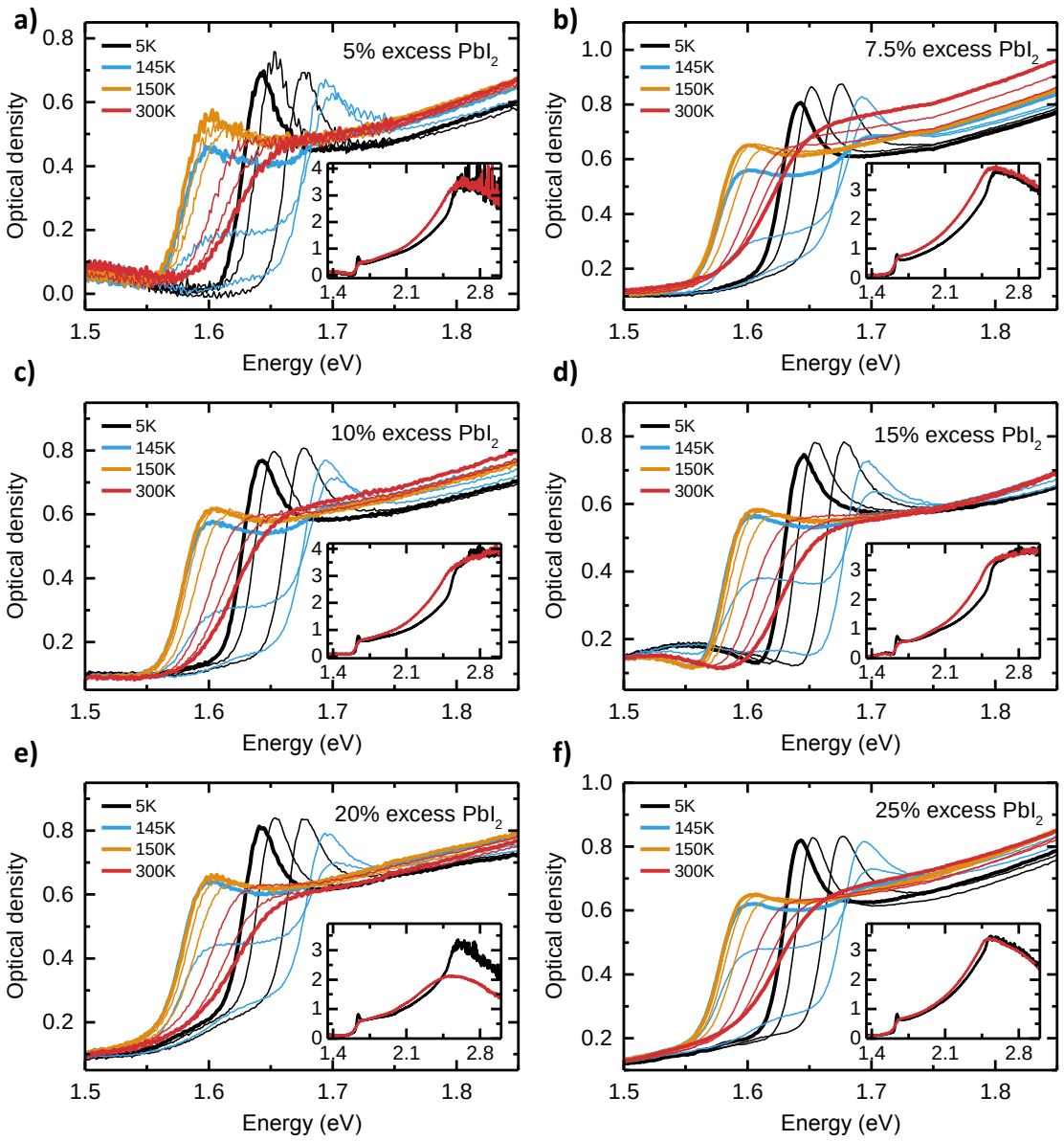

Figure S7 (a-f) Temperature dependent absorption spectra of $MAPbI_3$ thin films with different molar ratio of excess PbI_2 in the precursor solution as indicated. Thin lines without label correspond to the temperatures 260 K, 220 K, 180 K, 160 K, 140 K, 120 K, 80 K and 40 K. An appropriate offset correction was applied due to scattering effects.

Analysis of absorption spectra of $MAPbI_3$ with different grain sizes

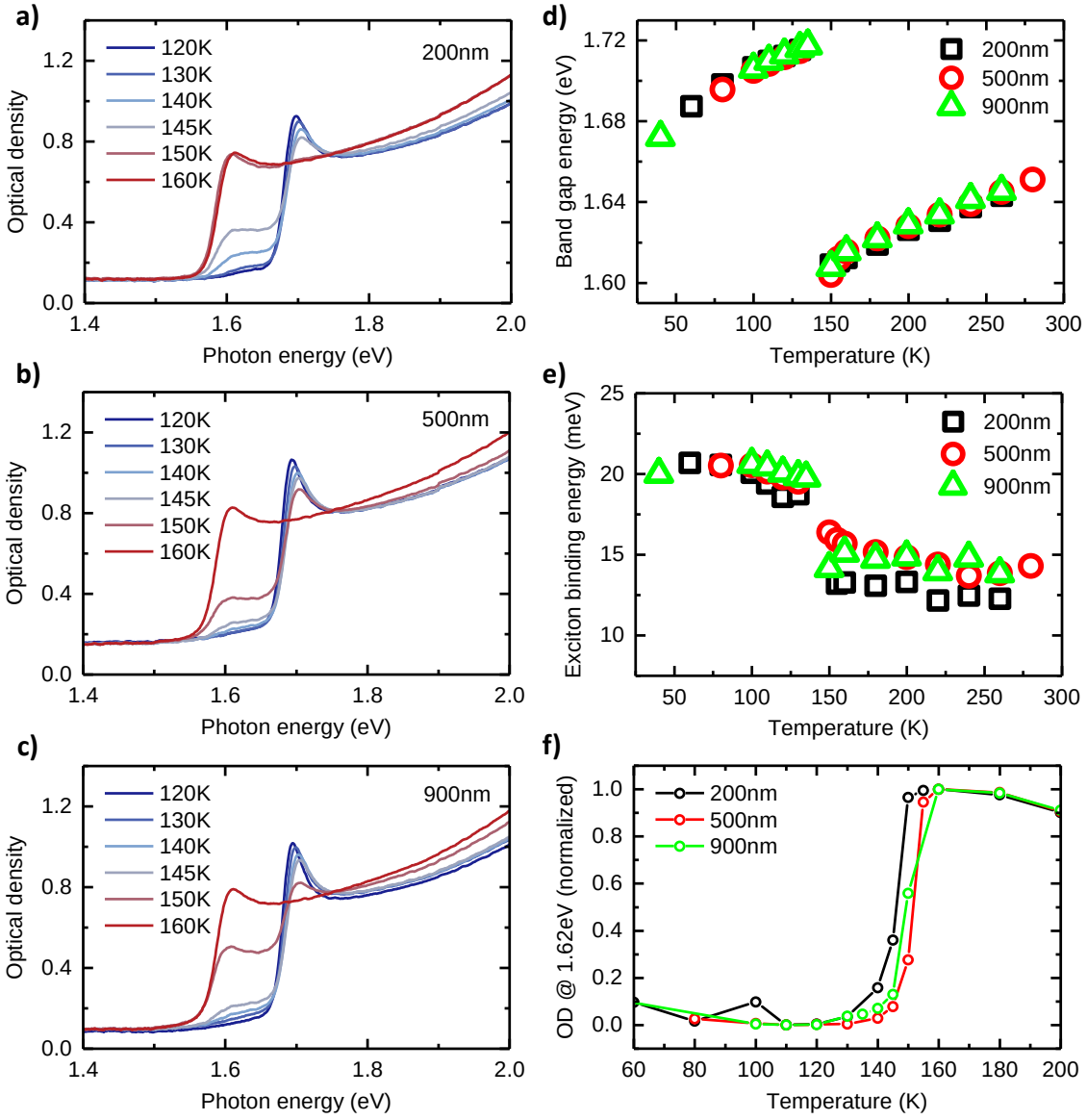

Figure S8 (a-c) Temperature dependent absorption spectra of $MAPbI_3$ samples with average grain sizes of 200 nm, 500 nm and 900 nm as indicated. Temperature dependent band gap energy (d) and exciton binding energy (e) extracted from fitting the temperature dependent absorption spectra with the model from Elliott for the samples with different grain size. (f) Normalized absorption coefficient at 1.62 eV photon energy as a function of temperature for the different grain sizes.

Table S4 Slope of the exciton binding energy in the temperature range 160 – 300 K and the phase transition temperature deduced from the point of inflexion in Figure S8f as a function of grain size.

Grain size (nm)	Linear temperature coefficient (10^{-5} eV/K)	Phase transition temperature (K)
200	-1.1 ± 0.4	146.5 ± 0.3
500	-1.4 ± 0.4	151.7 ± 0.2
900	-1.0 ± 0.5	150.5 ± 0.5

Modelling of the absorption coefficient in the framework of Elliott's theory

For fitting the measured absorption spectra we use the model derived by Elliott where the absorption as a function of photon energy is given by:[1]

$$\alpha(E) \propto \left[\sum_n \frac{2E_B}{n^3} \operatorname{sech}\left(\frac{E - E_g + \frac{E_B}{n^2}}{\Gamma} \right) + \int_{E_g}^{\infty} \operatorname{sech}\left(\frac{\varepsilon - E_g + \frac{E_B}{n^2}}{\Gamma} \right) \frac{1}{1 - e^{-2\pi \sqrt{E_B/(\varepsilon - E_g)}}} \mathrm{d}\varepsilon \right] \quad (1)$$

E, E_B, E_g, Γ, and μ are the photon energy, exciton binding energy, band gap energy, FWHM of the excitonic peak and the effective reduced mass.

The determination of the exciton binding energy through fitting in this framework is possible due to the different dependencies of bound and continuum states on the exciton binding energy. Therefore, the success of the fit depends on whether the bound states can be distinguished from the continuum contribution. At higher temperatures, when the excitonic character of the absorption onset in $MAPbI_3$ is less pronounced this might not

be the case. This leads to an increased uncertainty of the exciton binding energy. Figure S9 shows three different possible fits of the absorption spectrum of $MAPbI_3$ at 300 K. As indicated, the exciton binding energy varies in the range 12.9 – 17.7 meV. From this, we estimate the fitting uncertainty of the binding energy to be 2 meV for the entire temperature range. We note that though we have included a baseline correction in our model this does not account fully for scattering effects which appear below the band gap energy and the fitting uncertainty thus might be higher than assumed. The fitting range therefore was chosen in a way that the region below the band gap energy was truncated to reduce the influence of scattering effects.

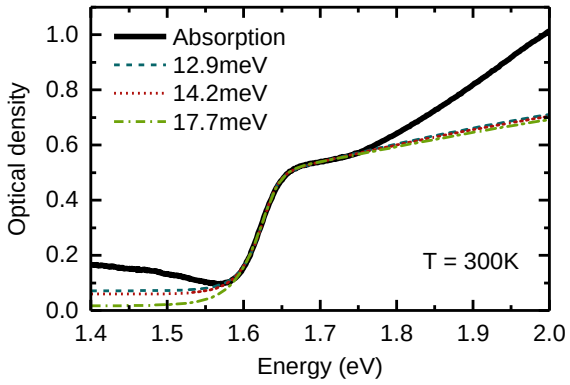

Figure S9 Fits of the absorption spectrum of $MAPbI_3$ at 300 K in the framework of Elliott's theory with different fitting ranges. The indicated values represent the exciton binding energy for the different fitting curves.

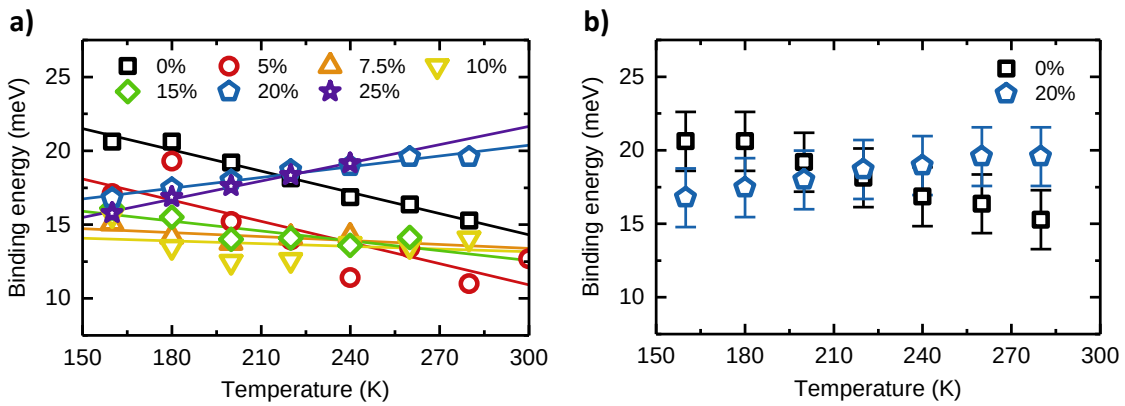

Figure S10 (a) Exciton binding energies as a function of temperature together with linear fits in the temperature range 160 – 300 K for the investigated samples with different degree of excess PbI_2 as indicated. (b) Values of the exciton binding energy for 0 % and 20 % excess PbI_2 samples alongside with fitting uncertainties.

Temperature dependence of dielectric constant in the tetragonal phase

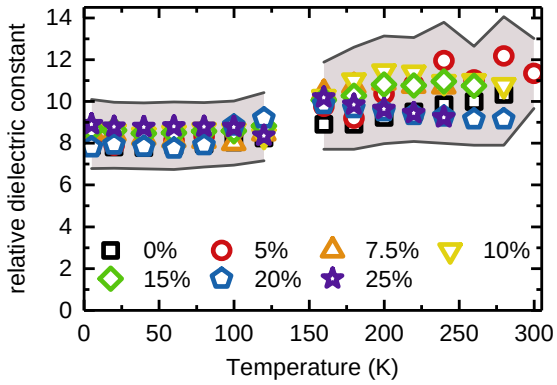

Figure S11 Temperature dependence of the relative dielectric constant of $MAPbI_3$ derived from the exciton binding energy for different excess PbI_2 content in the precursor solution alongside with the error margin marked in grey shading.

Calculation of temperature dependent unit cell volume

In course of the tetragonal to orthorhombic phase transition, the volume of the unit cell increases by about 5 %, which is the same amount compared to the reduction in volume due to the prior cooling of the sample from room temperature (975 $Å^3$) to 160 K (931 $Å^3$).

All considered values of the unit cell volume were taken from experimental data presented in the work from Baikie et al.[2]

The value of the unit cell volume at room temperature was taken from experimental data presented in Figure 9 in the work from Baikie et al. In this work the lowest temperature where the investigated sample is in its tetragonal phase was at 155 K. We therefore calculated the unit cell volume at 155 K, based on the given values of the lattice constants at that temperature which are a = c = 8.65 Å and b=12.45 Å thus leading to a unit cell volume at 155 K of 931 $Å^3$ which is about 5% less than 975 $Å^3$.

At 150 K the sample was found to have changed its crystal structure to an orthorhombic structure. The corresponding lattice constants at that temperature are a = 8.9 Å, b = 12.67 Å, c = 8.65 Å which yields a cell volume of 975 $Å^3$, equal to that at room temperature.

Supplementary References

1. S. Singh, C. Li, F. Panzer, K. L. Narasimhan, A. Graeser, T. P. Gujar, A. Köhler, M. Thelakkat, S. Huettner and D. Kabra, *J. Phys. Chem. Lett.*, 2016, **7**, 3014-3021.
2. T. Baikie, Y. Fang, J. M. Kadro, M. Schreyer, F. Wei, S. G. Mhaisalkar, M. Graetzel and T. J. White, *J. Mater. Chem. A*, 2013, **1**, 5628-5641.